Bouraba, A., Saighi, M., Saidani-Scott, H., & Hamidat, A. (2017). Cooling mechanisms of a solar assisted air conditioner: an investigation based on pressure-enthalpy chart. *International Journal of Refrigeration*, *80*, 274-291. https://doi.org/10.1016/j.ijrefrig.2017.05.008

Accepted Manuscript

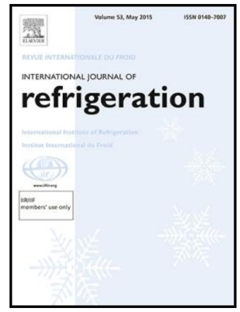

Title: Cooling mechanism of a solar assisted air conditioner: an investigation based on pressure-enthalpy chart

Author: Abdenour Bouraba, Mohamed Saighi, Hind Saidani-Scott, Abderrahmane Hamidat

PII: S0140-7007(17)30197-4
DOI: http://dx.doi.org/doi: 10.1016/j.ijrefrig.2017.05.008
Reference: JIJR 3639

To appear in: *International Journal of Refrigeration*

Received date: 10-11-2016
Revised date: 8-5-2017
Accepted date: 9-5-2017

Please cite this article as: Abdenour Bouraba, Mohamed Saighi, Hind Saidani-Scott, Abderrahmane Hamidat, Cooling mechanism of a solar assisted air conditioner: an investigation based on pressure-enthalpy chart, *International Journal of Refrigeration* (2017), http://dx.doi.org/doi: 10.1016/j.ijrefrig.2017.05.008.

Cooling mechanism of a solar assisted air conditioner: an investigation based on pressure-enthalpy chart

Abdenour Bouraba[1,2], Mohamed Saighi[2], Hind Saidani-Scott[3], Abderrahmane Hamidat[1]

[1]Centre de Développement des Energies Renouvelables (CDER), BP. 62, Route de l'Observatoire, Bouzaréah, 16340, Algiers, Algeria

[2](LTSE), University of Sciences and Technology Houari Boumediene (USTHB), BP. 32, Al-Alia, Bab Ezzouar, 16111, Algiers, Algeria

[3]Department of Mechanical Engineering, Queen's Building, University of Bristol, Bristol, UK

Corresponding author. Tel: +213 13189051; Fax: +213 180056

E-mail address : abdenourbourabaa@yahoo.fr, a.bourabaa@cder.dz

Highlights

- Cooling machine part of a solar-assisted air conditioner is investigated.
- Refrigerants considered are R-1234ze(E), R-134a and R410A.
- R-1234ze(E) yields the best performance in terms of discharge temperature.
- The system with R-1234ze(E) has higher gain than those with R-134a and R-410a.
- R-1234ze(E) yields higher *COP* augmentation than R-134a and R-410A.

Abstract

This paper reports a theoretical study of a conventional vapor compression air conditioner combined with a solar energy source. This system comprises two parts: the cooling mechanism and the solar heat source to operate it. Only the cooling machine part will be considered here, in which the refrigerant temperature leaving the immersed coil inside the storage tank can be calculated directly from the pressure-enthalpy diagram of the operating refrigerant. The investigation has been made using a new low global warming potential refrigerant that belongs to *HFO*'s family as an alternative to two high global warming potential refrigerants that belong to *HFC*'s family. These are R-1234ze(E) as an alternative to R-134a and R-410A. Comparisons between the classical vapor compression air conditioner and the solar assisted air conditioner and also between the selected refrigerants are investigated. The effect of the refrigerant temperature leaving the storage tank on the main performance parameters such as the coefficient of performance, the gain based on compression work, and the required condenser surface area are discussed.

Keywords:

Air conditioner

COP

Efficiency

Heat exchanger

Refrigerant

Nomenclature

A	Surface area *(m)*
c	Ratio of specific heats *(-)*
COP	Coefficient of performance *(-)*
c_p	Isobaric heat capacity $(kJ.kg^{-1}.K^{-1})$
c_v	Isochoric heat capacity $(kJ.kg^{-1}.K^{-1})$
d	Tube diameter *(m)*
G	Mass flux $(kg.m^{-2}.s^{-1})$
$gain$	Gain *(%)*
h	Specific enthalpy $(J.kg^{-1})$
k	Thermal conductivity $(W.m^{-1}.K^{-1})$
$lmtd$	Logarithmic mean temperature difference *(°C)*
m	Mass flow rate $(kg.s^{-1})$
Ntu	Number of transfer units *(-)*
P	Pressure *(Pa)*
P_r	Pressure ratio *(-)*
Pr	Prandtl number *(-)*
Q	Heat transfer rate (*W*)

Re_d	Reynolds number based on tube diameter *(-)*
T	Temperature *(°C)*
UA	Overall heat transfer coefficient $(W.K^{-1})$
w_{act}	Power required for actual compressor *(W)*
w_{is}	Power required for isentropic compressor *(W)*
Greek letters	
α	Heat transfer coefficient $(W.m^{-2}K^{-1})$
ε	Heat exchanger effectiveness *(-)*
η	Fin efficiency *(-)*
η_{is}	Compressor isentropic efficiency *(-)*
η_o	Surface efficiency *(-)*
μ	Viscosity $(\mu Pa.s)$
ρ	Density $(kg.m^{-3})$
Subscripts	
a	Air
act	Actual
a_1	Air inlet
a_2	Air outlet
conv	Conventional
d	Discharge
des	Desuperheat
i	Inner, inside
in	Inlet
is	Isentropic
l	Liquid
o	Outer, outside
r	Refrigerant
sat	Saturation
sol	Solar
sp	Single-phase
suc	Suction
tp	Two-phase
v	Vapor
1	Compressor entering state
2	Condenser entering state
2i	Ideal compressor exiting state
3	Condenser exiting state
3a	Desuperheated portion exiting state

4	Evaporator entering state
Superscripts	
e	Evaporator
c	Condenser

1. Introduction

The so-called vapor compression cycle was used for a long time in many applications of air conditioning and refrigeration systems. The performance of this cycle depends on many factors such as the condenser and the evaporator sizes, the degree of both subcooling and superheating, the refrigerant mass flow rate and the air flow rates through the condenser and the evaporator if finned tube heat exchangers are used. Bejan (1989), Klein (1992), Wu (1995), Wu et al. (1996) and Klein and Reindl (1998) among many others found that the refrigeration cycle performance is optimized at a point in which the condenser and the evaporator heat exchangers are approximately of equal size. Previous papers on the performance of the vapor compression systems showed that the critical temperature and the latent heat of vaporization are two key parameters that affect the coefficient of performance *COP*. According to Motta and Domanski (2000), the difference in *COP*s is related to different levels of irreversibility on the superheated-horn side and at the throttling process. The throttling-induced and superheated vapor-horn irreversibilities are affected by the slopes of saturation lines. They indicated that different refrigerants' critical temperatures and differences in the shape of the two-phase dome on the temperature-entropy diagram can explain different performance trends for the refrigerants studied. Thus, the general performance of the vapor compression system also depends on the type of refrigerant. From the beginning of the 19th century, a variety of refrigerants has been proposed for different refrigeration machines (Midgley and Henne, 1930; Benning and McHarness, 1939;

Hendricks, 1953). The majority of them were gradually replaced by better alternatives due to their serious effects on the climate change or human safety or both. For instance, the development history of several new compounds that may serve as alternatives can be found in the studies of McLinden and Didion (1988), Trepp et al. (1992), Devotta et al. (1993), Godwin (1994), Devotta (1995), Aisbett and Pham (1998), Calm and Didion (1998), Devotta et al. (2001), Spatz and Motta (2004), Calm (2008) and Bhatkar et al. (2013).

On the other hand, the development of technologies and the fast increase of population imposed a considerable demand in the conventional electrical source. In Algeria, buildings, with about 35% in the residential sector and 6% in the tertiary sector, use approximately 42% of total energy consumption (Missoum et al., 2014). One of the most important demands for electricity is related to the heating, ventilating and air conditioning systems. Perhaps, solar thermal energy appears as a good alternative among renewable energy sources that can be used to diminish our dependency on electricity production. Furthermore, the solar energy represents the heat source that is offered at a maximum temperature of 140°C by solar system collector.

Many applications of solar air collectors are reported in the work by Kalogirou (2004) while a paper by Henning (2007) reviews many issues for using solar thermal energy for air conditioner systems. Al-Alili et al. (2014) provided overviews for working principles of solar thermally operated cooling technologies and review for advancements of such technologies from the most recent publications. Methods of testing to determine the thermal performance of solar collectors including flat plate and vacuum tube are presented by Rojas et al. (2008) and Zambolin and Del Col (2010). Note that flat plate collectors generally operate in the temperature range 60°C-90°C are commonly in use but evacuated tube collectors are more appropriate for heating and cooling applications due to its ability to produce high temperatures (Arora et al., 2011). Since solar energy availability varies over the day and the seasons, its use mainly relies on the heat storage where the available energy is collected and stored so that it can be used when heat is needed. There are mainly three types of thermal energy storage systems (Dinçer and Rosen, 2011). These are sensible heat storage (Fernandez et al., 2010), latent heat storage (Sharma et al., 2009), and thermochemical storage (Michel et al., 2012). According to Tatsidjodoung et al. (2013), sensible heat storage method is the most widely used technique for heating and cooling needs because is the simplest and least expensive way to store energy. Recently, the combination of conventional vapor compression air conditioner system with any type of renewable energy becomes the subject of numerous studies (Bilgili, 2011; Ha and Vakiloroaya, 2012; Al-Alili et al., 2012; Vakiloroaya et al., 2013; Ha and Vakiloroaya, 2015).

This paper presents the general performance of conventional vapor compression air conditioner system combined with a solar energy source. This system comprises two parts: the cooling mechanism and the solar heat source to operate it. Only the cooling machine part will be considered here, while the refrigerant temperature leaving the immersed coil inside the storage tank can be calculated directly from the pressure-enthalpy diagram. The refrigerants considered are R-134a, R-410A and R-1234ze(E). It is well-known that R-134a and R-410A are non-toxic, non-inflammable and have zero ozone depleting potential, *ODP*=0, but their greenhouse warming potential is very significant, *GWP*=1430 for R-134a and *GWP*=2088 for R-410A (Bitzer, 2014). According to Devotta et al. (2001), only refrigerants with zero ozone depletion potential are considered for air conditioners.

Internationally, the production and the use of *HFCs*, such as R-134a, and their mixtures, including R-410A, are now aimed by the international environmental agreements (Bitzer, 2014; EU, 2014). Hence, the fourth generation fluorinated refrigerant gases known as *HFO*s are currently selected as the best alternatives that are safe for both the users and the environment, see Minor and Spatz (2008), Leck (2009, 2010), Motta et al. (2010), Karber et al. (2012), Pham and Rajendran (2012), Esbri et al. (2013), Babiloni et al. (2014) and Aprea et al. (2016). Similar to *HFC*s, these refrigerants contain hydrogen, fluorine and carbon but they have very short atmospheric lifetimes of a few days. It is well known that R-1234yf belongs to the *HFO*'s family and characterized by zero *ODP* and very low *GWP*, as low as 4, as reported by Nielsen et al. (2007), Minor and Spatz (2008) and Papadimitriou et al. (2008). It has vapor pressure and other properties similar to R-134a which can be used for progressive elimination of refrigerants with high *GWP* in mobile air-conditioning systems (Bryson et al., 2011). R-1234ze is intended to replace R-134a and R-410A in residential and commercial air conditioning while offering a 75% reduction in *GWP* (Ansari et al., 2013; Janicki et al., 2014).

2. Procedure

This paper provides a theoretical technique to be used in determining the general performance of a conventional vapor compression system combined with solar collector. The refrigerant leaving the compressor, as superheated vapor, goes through immersed coil inside the storage tank. A part of the heat received from the solar collector is used to heat the superheated vapor at constant volume until the condensation pressure of the conventional system is achieved. As the refrigerant temperature leaving the storage tank increases by increasing solar collector temperature, the compressor discharge temperature and its corresponding pressure decreased. The discharge temperature can be calculated by an equation derived from the pressure-enthalpy diagram. However, the discharge pressure can be calculated by assuming the superheated vapor as an ideal gas. The mathematical procedure applied to the classical vapor compression cycle will then be used for this new cycle, just introducing some modifications during the compression process.

3. Conventional vapor compression cycle

The general diagram of a vapor compression machine shown in Fig. 1 consisted of four major components: finned tube condenser, fin-and-tube evaporator for cooling air, a compressor and an expansion device.

3.1. Coefficient of performance

The coefficient of performance, *COP*, is defined as the ratio between the refrigeration capacity (Q^e) and the power required by the compressor (w_{act}), that is:

$$COP = \frac{Q^e}{w_{act}} = \left(\frac{Q^c}{Q^e} - 1\right)^{-1} \tag{1}$$

Where, superscripts *e* and *c* refer to evaporator and condenser, respectively, and Q^c is the rate of heat transfer from the condenser to the ambient given by:

$$Q^c = Q^e + w_{act} \tag{2}$$

The maximum possible *COP* for a refrigerator operating between a lower temperature and an upper temperature is achieved by a reversible Carnot refrigeration cycle as illustrated in Fig. 2. Here, the cycle is indicated without sub-cooling and superheating. The second law requires that (Tobin, 1969) :

$$\frac{Q^c}{T^c_{sat}} = \frac{Q^e}{T^e_{sat}} \tag{3}$$

Where, T_{sat}^{e} and T_{sat}^{c} are the evaporating and the condensing temperatures, respectively. Substituting Eq. (3) into Eq. (1), the Carnot *COP* can be obtained as:

$$COP_c = \left(\frac{T_{sat}^{c}}{T_{sat}^{e}} - 1\right)^{-1} \quad (4)$$

Leff (1987) reported that the Carnot efficiency is a relatively poor guide to the efficiencies of real engines. He said that real engines do not generally operate isothermally at the highest and lowest temperatures of the cycle. Rather, they absorb and reject heat along variable temperature paths. Therefore, the temperature distributions of the heating fluid and the cooling fluid are not constant throughout the heat exchangers. As shown in Fig. 2, the Carnot *COP* was based on the air inlet temperatures to the heat exchangers $T_{a_1}^{e}$ and $T_{a_1}^{c}$. According to McQuiston and Parker (1982), the *COP* is closely related to the evaporating and condensing temperatures. For the highest *COP* the cycle should be operated at the lowest possible condensing temperature and the highest possible evaporating temperature. In the present investigation, all *COP*s were calculated according to Eq. (1).

3.2. System modeling

This section describes the derived mathematical models for the mean components of the conventional vapor compression air conditioner system.

3.2.1. Compressor

The objective of the compressor is to increase the working pressure of the refrigerant. Among different types of compressors, Chen et al. (2002) reported that the scroll type positive displacement compressors are the most used type in small and medium sized air conditioning systems. The power requirement for a non-ideal compressor is given by:

$$w_{act} = \frac{w_{is}}{\eta_{is}} = m_r(h_2 - h_1) \tag{5}$$

In which, h is the specific enthalpy, m_r is the refrigerant mass flow rate, w_{is} is the isentropic compression work and η_{is} is the isentropic efficiency. The power required for isentropic compression is given by the following expression (Cleland, 1986):

$$w_{is} = \frac{c-1}{c} P_{suc} v_1 \left(\left(\frac{P_{dis}}{P_{suc}} \right)^{\frac{c-1}{c}} - 1 \right) = m_r(h_{2i} - h_1) \tag{6}$$

Where, c is the compression index, h_{2i} is the ideal specific enthalpy of refrigerant exiting the compressor, P_{suc} is the suction pressure (evaporating pressure for the conventional cycle), P_{dis} is the discharge pressure (condensing pressure for the conventional cycle) and v_1 is the suction volume. The compressor isentropic efficiency is calculated as follows:

For R-134a (Brown et al., 2002):

$$\eta_{is} = 0.9343 - 0.04478 P_r \tag{7}$$

Where, P_r is the ratio of condensing pressure to evaporating pressure.

For R-410A (Lottin et al., 2003):

$$\eta_{is} = 0.0093P_r^2 - 0.1023P_r + 0.8429 \tag{8}$$

In the case of R-1234ze(E), no correlation for the isentropic efficiency is available in the literature at the time of writing. Motta et al. (2010) found that the isentropic efficiency of R-1234ze(E) compressor is 18% lower than that for R-134a compressor. Other investigators assumed a constant isentropic efficiency (Ansari et al., 2013; Meng et al., 2016). In the present paper, the isentropic efficiency of R-1234ze(E) will be calculated by the following equation (Radcenco et al., 1995):

$$\eta_{is} = \frac{T_{d,is} - T_1}{T_{d,act} - T_1} = \frac{h_{d,is} - h_1}{h_{d,act} - h_1} \tag{9}$$

In which, $T_{d,is}$ is the ideal compressor discharge temperature and $T_{d,act}$ is the actual compressor discharge temperature. Note that for a conventional system shown in Fig. 1, $T_{d,is} = T_{2i}$ and $T_{d,act} = T_2$.

3.2.2. Condenser

The condenser used in this work is a cross-flow air-refrigerant type, in which refrigerant flows inside tubes while air flows between fins and tubes. Considering the steady state model of the vapor compression cycle, the heat transfer rate from the air-stream to the fin-and-tube condenser is:

$$Q^c = (\varepsilon c_{min})^c \left(T_{r,in} - T_{a_1}\right)^c \tag{10}$$

Where, c_{min} is the minimum capacitance rate between that of the air and the refrigerant, T_{a_1} is the air inlet temperature to the condenser and $T_{r,in}$ is the refrigerant temperature at the condenser inlet. Assuming no extraneous heat leaks, an energy balance for the air-stream will yield:

$$Q^c = \left(m_a c_{p,a}\right)^c \left(T_{a_2} - T_{a_1}\right)^c \tag{11}$$

Here, m_a and $c_{p,a}$ are the mass flow rate and the specific heat capacity of the air stream and T_{a_2} is the air temperature leaving the heat exchanger. Although the refrigerant enters the condenser as a superheated vapor and leaves it as subcooled liquid, the condenser can be divided into de-superheated, saturated, and subcooled sections, Fig. 3. The hypothesis that no extraneous heat leaks is again considered, thus:

$$Q^c = Q^c_{des} + Q^c_{tp} + Q^c_{sub} \tag{12}$$

where

$$Q^c_{des} = m_r(h_2 - h_{3a}) \tag{12a}$$

$$Q^c_{tp} = m_r(h_{3a} - h_{3b}) = m_r h^c_{fg} \tag{12b}$$

$$Q^c_{sub} = m_r(h_{3b} - h_3) \tag{12c}$$

Where, h_{fg} is the latent heat of condensation. In addition, the steady rate of heat flow from the refrigerant to the ambient air can be calculated by the log mean temperature difference method:

$$Q^c = (UA)^c lmtd^c \tag{13}$$

If the source and the sink are isothermal, the heat transfer Q^c flows from the hot refrigerant to the air across a temperature difference $\left(T_{sat} - T_{a_1}\right)^c$. In this case, Bejan (1989) and Klein (1992) assumed that the overall heat transfer coefficient area product $(UA)^c$ is the product of the heat exchanger effectiveness ε^c, and the minimum capacitance rate c_{min}^c , i.e.

$$(UA)^c = (\varepsilon C_{min})^c \tag{14}$$

Here, the air temperature varies through the condenser flow length and the heat conductance is given by combining Eq. (10) and Eq. (13) as:

$$(UA)^c = (\varepsilon C_{min})^c \frac{\left(T_{r,in} - T_{a_1}\right)^c}{lmtd^c} \tag{15}$$

Where, the log mean temperature difference is given by:

$$lmtd^c = \frac{Q^c}{\frac{Q_{des}^c}{lmtd_{des}^c} + \frac{Q_{tp}^c}{lmtd_{tp}^c} + \frac{Q_{sub}^c}{lmtd_{sub}^c}} \tag{16}$$

in which

$$lmtd_{des}^c = \frac{\left(T_{sat} - T_{a_1}\right)^c - \left(T_{r,in} - T_{a_2,des}\right)^c}{ln \frac{\left(T_{sat} - T_{a_1}\right)^c}{\left(T_{r,in} - T_{a_2,des}\right)^c}} \tag{17a}$$

$$lmtd_{tp}^{c} = \frac{\left(T_{sat}-T_{a_2,tp}\right)^{c}-\left(T_{sat}-T_{a_1}\right)^{c}}{ln\frac{\left(T_{sat}-T_{a_2,tp}\right)^{c}}{\left(T_{sat}-T_{a_1}\right)^{c}}} \tag{17b}$$

$$lmtd_{sub}^{c} = \frac{\left(T_{r,out}-T_{a_1}\right)^{c}-\left(T_{sat}-T_{a_2,sub}\right)^{c}}{ln\frac{\left(T_{r,out}-T_{a_1}\right)^{c}}{\left(T_{sat}-T_{a_2,sub}\right)^{c}}} \tag{17c}$$

Where, $T_{a_2,des}$ and $T_{a_2,tp}$ are the air temperature leaving the desuperheated and the two phase portions given by assuming no extraneous heat losses:

$$T_{a_2,des}^{c} = \frac{Q_{des}^{c}}{\left(m_a c_{p,a}\right)^{c}} + T_{a_1}^{c} \tag{18a}$$

$$T_{a_2,tp}^{c} = \frac{Q_{tp}^{c}}{\left(m_a c_{p,a}\right)^{c}} + T_{a_1}^{c} \tag{18b}$$

$$T_{a_2,sub}^{c} = \frac{Q_{sub}^{c}}{\left(m_a c_{p,a}\right)^{c}} + T_{a_1}^{c} \tag{18c}$$

Furthermore, the overall heat transfer resistance can also be evaluated from the following relationship:

$$(UA)^{c} = \left(\frac{1}{(\propto_o A_o)^{c}} + \frac{1}{(\propto_i A_i)^{c}}\right)^{-1} \tag{19}$$

Where, A_o is the required external surface area, A_i is the tube inside area, $\propto_i$ is the inside tube heat transfer coefficient and $\propto_o$ is the design coefficient. The design coefficient can be related to the actual fin side heat transfer coefficient $\propto_o^{''}$ and the finned surface effectiveness η_o as:

$$(\propto_o)^{c} = \left(\eta_o \propto_o^{''}\right)^{c} \tag{19a}$$

The finned surface effectiveness may be written in terms of the fin efficiency η, fin surface area A_f and the total external area A_o as:

$$\eta_o^c = \left(1 - \frac{A_f}{A_o}(1-\eta)\right)^c \tag{19b}$$

For staggered plate-fin geometry, the fin efficiency can be calculated analytically using the approximation from Hong and Webb (1996). The temperature of the refrigerant leaving the subcooled region is given by:

$$T_{r,out}^c = T_3 = T_{sat}^c - \Delta T_{sub} \tag{20}$$

Furthermore, the calculation of the fin-side and the tube-side heat transfer coefficients will be discussed later in the section on the condenser heat transfer coefficients. In addition, the calculation of the exchanger effectiveness will also be discussed later in the section on heat exchanger effectiveness.

3.2.3. Throttling

The throttling process reduces the refrigerant pressure from the high pressure to the low pressure. The energy equation shows that the expansion process is isenthalpic, then:

$$h_3 = h_4 \tag{21}$$

3.2.4. Evaporator

The analysis of the parameters of the evaporator is almost identical to that of the condenser. However, the dehumidification process implies some modifications. The refrigerant entering the evaporator absorbs heat from warm indoor air and is heated above the saturation temperature before entering the compressor. The indoor air is cooled and dehumidified as it flows over the evaporator and returned to the living space. If the dew point temperature of the moist air entering the evaporator is higher than the coil surface temperature, water vapor in the entering air will be condensed and then the condensate will be trained out. Moreover, the condensate retained on the heat exchanger surface has hydrodynamic effects by changing the surface geometry and the air flow pattern (Bourabaa et al., 2011). Since the evaporator is not the focus of this paper, only information such as cooling capacity and inlet and outlet enthalpies are needed to determine the required refrigerant mass flow rate.

For a given cooling capacity, the mass flow rate of the refrigerant passing through the evaporator is calculated by:

$$m_r = \frac{Q^e}{h_1 - h_4} = \frac{Q^e}{\Delta h^e} \tag{22}$$

3.3. Heat exchanger effectiveness

Due to the desuperheating and subcooling regions in the most typical condensers, the refrigerant undergoes a larger temperature change than the air. In this case, the following expression can be used to calculate the effectiveness for a cross-flow heat exchanger with both fluids unmixed:

$$\varepsilon^c = 1 - exp\left(\left(\frac{Ntu^{0.22}}{c_{rat}}\right)\left(exp(-c_{rat}Ntu^{0.78}) - 1\right)\right) \tag{23}$$

Where, c_{rat} is the ratio of the minimum heat capacitance to the maximum heat capacitance and Ntu is the number of transfer units. In the saturated portion of the condenser, it is more common to define the effectiveness as if the air would undergoes a larger temperature difference. In this case, the minimum heat capacitance is that of the air, thus:

$$\varepsilon^{c} = \frac{Q^{c}}{\left(m_a c_{p,a}\right)^{c}\left(T_{sat} - T_{a_1}\right)^{c}} \tag{24}$$

Furthermore, if the heat conductance $(UA)^{C}$ is known, the condenser effectiveness can be given by the following expression (London and Seban, 1980):

$$\varepsilon^{c} = 1 - exp\left(-\frac{UA}{m_a c_{p,a}}\right)^{c} \tag{25}$$

In evaporators, since the superheating zone is very small relative to the two-phase region, the evaporator effectiveness can be expressed as:

$$\varepsilon^{e} = 1 - exp\left(-\frac{UA}{m_a c_{p,a}}\right)^{e} \tag{26}$$

A special case is encountered when the heat source and the heat sink are isothermal, Klein (1992) reported that the refrigeration cycle is optimized at $(UA)^{C} = (UA)^{e}$, and the evaporator effectiveness can be deduced directly by the following equation:

$$\varepsilon^{e} = \varepsilon^{c} \frac{\left(m_a c_{p,a}\right)^{c}}{\left(m_a c_{p,a}\right)^{e}} = \frac{(UA)^{e}}{\left(m_a c_{p,a}\right)^{e}} \tag{26a}$$

As mentioned previously, the distributions of the refrigerant in the heat sink (air) and heat source (also air) are not constant throughout the heat exchangers. Therefore, the evaporator effectiveness can be calculated by assuming that the air undergoes a larger temperature change along the heat exchanger, i.e.:

$$\varepsilon^e = \frac{(Q)^e}{(m_a c_{p,a})^e (T_{a_1 - T_{sat}})^e} \tag{26b}$$

3.4. Refrigerant properties

Thermodynamic properties, such as density, thermal conductivity, viscosity, isobaric heat capacity and specific enthalpy for both liquid and vapor states, of R-134a and R-410A can be measured using specified correlations as those by Kabelac (1991), Cleland (1994), Lemmon (2003), Küçüksille et al. (2009) and Küçüksille et al. (2011). It must be noted that R-410A has a very slight temperature glide (<1°*C*), in which the dew point and bubble point temperatures may be ignored. In this paper, the fundamental thermodynamic properties (including thermodynamic properties and transport properties) of R-134a and R-410A are calculated from Reference Fluid Thermodynamic and Transport Properties REFPROP.8 (Lemmon et al., 2007). For R-1234ze(E), the method given by Thol and Lemmon (2016) is applied. In this method, the refrigerant heat capacity and the refrigerant enthalpy for both liquid and vapor states can be calculated through the use of the derivatives of the Helmholtz energy equation (Appendix A). The calculation of other properties such as density, viscosity and thermal conductivity for both liquid and vapor phases are also presented in Appendix A. Typical properties of the selected refrigerants are summarized in Table 1.

4. Vapor compression air conditioner combined with solar collector

Fig. 4 shows a general diagram of an air conditioner machine in which the conventional vapor compression system is combined with a vacuum solar collector. In this new system, the refrigerant leaving the compressor is partially compressed. The rest of the compression is made, by thermal way, at constant volume (constant volume line *2a*-*2b* in Fig. 5). Note that the *P*-*h* diagram in Fig. 5 is for R-1234ze(E) generated by Akasaka (2010) using the extended corresponding state (ECS) model established by Leland and Chappelear (1968). The compressor outlet temperature at the state *2a* must be on the line *1*-*2i* for isentropic compression or on the line *1*-*2* for actual compression. The compressor discharge temperature reaches its maximum value at state *2i* (or state *2*), which corresponds to the conventional vapor compression cycle. However, its minimum value is at the point *2a*, which is on the same constant volume line with the maximum temperature that can be reached by the energy source (line *2a*-*2b*). Hence, at any refrigerant temperature leaving solar collector, state *2b'*, the compressor discharge temperature can be approximated by the following expression:

$$T_{2a'} = T_2 - \frac{T_2 - T_{2a}}{T_{2b} - T_2}(T_{2b'} - T_2) \qquad (27)$$

For a given T_{2b}, the corresponding compressor outlet temperature, T_{2a}, is taken directly from the pressure-enthalpy diagram, while T_2 is the compressor outlet temperature in the conventional vapor compression cycle.

The gain based on the compressor work is defined as the ratio of the difference between the mechanical compression between state *1* and state *2* (w_{conv}) and the mechanical compression between state *1* and state *2a* (w_{sol}) to the mechanical compression between state *1* and state *2* (w_{conv}) as shown in Fig. 5. This can be expressed as:

$$Gain = \frac{w_{conv} - w_{sol}}{w_{conv}} \times 100 \tag{28}$$

5. Condenser heat transfer coefficients

In this section, the heat transfer coefficients through a finned tube condenser are briefly presented.

5.1. Tube-side

For single phase-flow, the following equation can be used (Saechan and Wongwises, 2008):

$$\propto_i = \propto_{sp} = a \frac{k}{d_i} Pr^{1/3} Re_{d_i}^{1+b} \tag{29}$$

Where, d_i is the tube inner diameter, k is the refrigerant thermal conductivity, Re_{d_i} is the Reynolds number based on inner diameter and Pr is the Prandtl number. Parameters a and b are:

$$Re_{d_i} < 3500, \qquad a = 1.10647, \qquad b = -0.78992$$
$$3500 \le Re_{d_i} \le 6000, \qquad a = 3.5194 \times 10^{-7}, \qquad b = 1.03804$$
$$6000 < Re_{d_i} \qquad a = 0.2243 \qquad b = -0.385$$

Because R-134a and R-1234ze(E) are known as pure compounds, the condensing heat transfer coefficient is calculated using the correlation by Shah (2009). This equation is the same as that in the Shah (1979) correlation except that the Shah (1979) correlation did not have the viscosity ratio factor. In horizontal tubes, this correlation uses two heat transfer equations:

$$\propto_I = \propto_l \left(\frac{\mu_l}{\mu_v}\right)^n \left[(1-x)^{0.8} + \frac{3.8x^{0.76}(1-x)^{0.04}}{P_{red}^{0.38}}\right] \tag{30a}$$

and

$$\propto_{Nu} = 1.32 Re_{ls}^{-1/3} \left(\frac{\rho_l(\rho_l-\rho_v)gk_l^3}{\mu_l^2}\right)^{1/3} \tag{30b}$$

Where, $n = 0.0058 + 0.557P_{red}$, P_{red} is the reduced pressure, Re_{ls} is the Reynolds number assuming liquid phase flowing alone, x is the vapor quality, and $\propto_l$ the liquid only heat transfer coefficient calculated from the correlation of Dittus and Boelter (1985):

$$\propto_l = 0.0241 \frac{k}{d_i} Re_{d_i}^{0.8} Pr^{0.4} \tag{31}$$

Hence,

For: $J_g \geq 0.98(Z + 0.263)^{-0.62}$, where $Z = \left(\frac{1}{x} - 1\right)^{0.8} Pr^{0.4}$, the following equation will be used:

$$\propto_{tp} = \propto_I \tag{32a}$$

For: $J_g < 0.98(Z + 0.263)^{-0.62}$ and $Re_{d_i} > 3.5 \times 10^4$ the following equation is recommended:

$$\propto_{tp} = \propto_I + \propto_{Nu} \tag{32b}$$

The dimensionless vapor velocity J_g is defined as:

$$J_g = \frac{xG_r}{[gd_i\rho_v(\rho_l - \rho_v)]^{0.5}} \tag{33}$$

Where, g is the acceleration due to gravity and G_r is the refrigerant mass flux.

For refrigerant mixtures such as R-410A, Bivens and Yokozeki (1994) have modified the Shah's empirical equation as:

$$\propto_i = \propto_{tp,mix} = F \propto_{tp} \tag{34}$$

Where, the empirical factor F is a function of the refrigerant mass flux G_r, and is given by:

$$F = 0.78738 + 6187.89 G_r^{-2} \tag{35}$$

5.2. Air-side

The fin-side heat transfer coefficient for dry fin-and-tube heat exchanger having plain fin geometry with multiple rows of staggered tubes can be calculated in terms of the non-dimensional Colburn j-factor as (Bourabaa et al., 2011):

$$\propto_o'' = jG_{a,max} c_{p,a} Pr^{-2/3} \tag{36}$$

In which, $G_{a,max}$ is the mass flux of the air based on the minimum flow area and the Colburn j-factor for fin-and-tube heat exchanger having plain fin pattern can be obtained from the correlation by Wang et al. (1996):

$$j = 0.394 Re_{d_o}^{-0.392} \left(\frac{t}{d_o}\right)^{-0.0449} N_r^{-0.0897} \left(\frac{F_p}{d_o}\right)^{-0.212} \quad (37)$$

Where, d_o is the tube outer diameter, F_p is the fin pitch, N_r is the number of tube rows, Re_{d_o} is the Reynolds number based on the outer tube diameter and t is the fin thickness. Moreover, correlations from McQuiston (1980), Webb (1980), Rabas et al. (1981), Abu Madi et al. (1998) and Wang et al. (2000) can be used to establish the air side heat transfer coefficient for various fin patterns.

6. Condenser geometry

In the application of the basic heat transfer data to the geometry of the fin-and-tube condenser, certain geometrical relationships are necessary. Kayansayan (1994) reported expressions that provide the geometrical description for a plate-fin, cross flow heat exchanger with staggered tube layout, see appendix B. Besides, the geometric parameters of the present fin-and-tube heat exchanger are illustrated in Table 2.

7. Results and discussion

The performance of a conventional vapor compression air conditioner machine having 3.517 kW will be firstly considered. The following conditions, such as condensing and evaporating temperatures (0°C and 40°C, respectively) and air mass flow rates ($m_a^e = 0.24\ kg.s^{-1}$ and $m_a^c = 0.64\ kg.s^{-1}$), are assumed constants. Assuming also that the cycle operates with a same value of subcooling and superheating ($5°C$). The refrigerants considered are R-134a and R-1234ze(E) as pure refrigerants, and R-410A as a refrigerant mixture. Under the same operating conditions, the study will then be extended to investigate the performance of the hybrid solar assisted air conditioner that consists of a vacuum solar collector and a conventional vapor compression air conditioner.

7.1. Conventional vapor compression air conditioner

Table 3 reports values of the main variables and parameters for the conventional vapor compression cycle. The refrigerant mass flow rates are calculated from the evaporator information such as heat capacity and, inlet and outlet enthalpies. Because the latent heat of vaporization h_{fg}^{e} differs for each refrigerant, the mass flow rates of the refrigerants are not similar for the same capacity condition. As well known, lower latent heat of vaporization leads to a higher refrigerant mass flow rate through the evaporator. The results here are consistent with this postulate in which, R-1234ze(E) has a higher mass flow rate than R-410A and R-134a because its latent heat of vaporization is the lowest. Note that, in the evaporator, the incoming liquid is not saturated liquid. Therefore, the refrigerant mass flow rate can be related to the difference between the evaporator inlet and outlet enthalpies Δh^{e} rather than to the latent heat of vaporization.

The discharge temperature of R-1234ze(E) is lower than that of R-134a, which in turn is lower than that of R-410A. This can be attributed to the losses due to superheat and throttling processes which depend very much on the slopes of saturation curves on the temperature-entropy diagram. For R-410A, both the superheat and throttling losses are significant which means that the deviation of the vapor compression cycle from the Carnot cycle could be significant. As a consequence, its operating cycle will be away from the vapor curve and thus a higher discharge temperature can be observed for this refrigerant. R-1234ze(E), having the smallest slope, has the lowest superheat losses, thus its compressor exit temperature will be very close to the condensing temperature.

The Carnot cycle operating between the evaporating and the condensing temperatures has the same coefficient of performance which doesn't depend on the working fluids ($COP_c=6.83$). In fact, the system working with R-1234ze(E) offers the best *COP* value, while R-410A offers the lowest *COP* value. It is obvious that the critical temperature and the latent heat of vaporization are two key thermodynamic parameters that affect the coefficient of performance. A cycle using R-1234ze(E) operates further from its critical point than R-134a and much further than R-410A. Thus, many researchers postulate that a fluid with a lower critical temperature will tend to have a lower coefficient of performance. According to Motta and Domanski (2000) the difference in *COP*s is related to different levels of irreversibility on the superheated-horn side and at the throttling process. The throttling-induced and superheated vapor-horn irreversibilities are affected by the slopes of saturation lines. These losses are greater near critical temperature where the saturation lines gradually become flatter to close the two-phase dome. The superheated vapor-horn irreversibility and throttling-induced irreversibility are greater for R-410A than for R-1234ze(E) and R-134a because it has lower critical temperature.

The power required for both the isentropic and the actual compressions is lower for R-1234ze(E) than that for R-134a, which in turn is lower than that for R-410A. This is because the refrigerant enthalpy of R-1234ze(E) at the evaporator inlet is slightly lower than that of R-134a, which in turn is lower than that of R-410A. For simplicity, lower refrigerant enthalpy entering the evaporator tends to decrease the compression work.

In condensers, the amount of the heat transfer rate can strongly affects the heat exchanger size. Under the same conditions, the condenser working with R-1234ze(E) needs a lower tube length, other geometrical parameters being kept constant. This is because the amount of the rejected heat through the condenser is the lowest compared to R-134a and R-410A.

7.2. Vapor compression air conditioner with solar collector

The main performance parameters, such as coefficient of performance, gain based on the compression work, isentropic and actual discharge temperatures and its corresponding pressures, power required for isentropic and actual compressors, and condenser surface augmentation, for a conventional vapor compression cycle combined with a solar collector are tabulated in Table 4. For all refrigerants, both the discharge temperature and the discharge pressure are lowered. As well known, the compressor discharge temperature is used as a criterion in considering suitability of use. Higher compressor discharge temperature may reduce the compressor life. On the other hand, lower discharge temperature ensures better R-1234ze(E) compressor life compered to R-134a and R-410A compressors. Therefore, the system with R-1234ze(E) is better than that with R-134a, which in turn is better than that with R-410A in terms of discharge temperature. In comparison with the conventional vapor compression system, the isentropic discharge temperature for R-134a is lowered by 14.3%, while the actual discharge temperature is lowered by 14.9%. For R-410A, the discharge temperature of the ideal compressor is lowered by 10.4%, while the actual discharge temperature is lowered by about 11%. For R-1234ze(E), the isentropic discharge temperature is lowered by 14.5%, while the actual discharge temperature is lowered by 15.1%. This means that the system with R-1234ze(E) is also better than that with R-134a, which in turn is better than that with R-410A in terms of discharge temperature degradation.

The discharge pressure for ideal compressor is slightly lower than that for a real compressor. This can be attributed to the intersection of the compression lines with the constant volume line on the pressure-enthalpy diagram.

The results showed that the combination of the conventional vapor compression air conditioner with solar energy source reduces its power consumption and increases its coefficient of performance. At the same value of the refrigerant temperature leaving the storage tank, the system with R-1234ze(E) yields the highest value of *COP* augmentation, while R-410A yields the lowest value. This implies that the *COP* improves more for a system with R-1234ze(E) than that with R-134a and R-410A.

Also, a slightly larger condenser is used to reject the additional heat amount obtained from the hot water in storage tank. The system with R-1234ze(E) needs higher surface augmentation than that with R-134a and R-410A. This can be related to the additional heat amount obtained from the water storage tank. It must be noted that refrigerants with lower discharge temperature, higher mass flow rate and higher vapor specific heat tend to have higher heat transfer rate.

As can be seen, the isentropic efficiency increased slightly than that for conventional systems because the pressure ratio decreases. It is well known that the isentropic efficiency varies with compressor suction and discharge conditions. From the pressure-enthalpy diagram, only the compressor discharge conditions vary with the variation of the refrigerant temperature leaving immersed coil, while the compressor suction conditions are kept constant.

The gain based on compression work is higher for a system with R-1234ze(E) than that with R-134a, which is higher than that with R-410A, and this indicates that R-1234ze(E) low *GWP* refrigerant would be a better choice for a solar assisted air conditioner in order to diminish our dependency on the electricity production.

7.3. Effect of refrigerant temperature leaving storage tank

The effects of variations in the refrigerant temperature leaving the immersed coil inside storage tank on the *COP* augmentation and also on the gain based on the compressor power input, are illustrated in Fig. 6 and Fig. 7, respectively. For more accuracy, the refrigerant temperature is defined as the dimensionless term: see Fig. 5.

$$\theta = \frac{T_{2b'} - T_2}{T_{2b} - T_2} \tag{38}$$

As can be seen, both the *COP* augmentation and the gain based on compression work increase with increasing refrigerant temperature leaving storage tank. The *COP* augmentation for a system with R-1234ze(E) increases more rapidly than those with R-134a and R-410A. This means that the *COP* improves more for R-1234ze(E). Similar trends are observed for the variation of the gain based on the compression work. As the refrigerant temperature leaving storage tank increases, the departure of the gain and *COP* augmentation profiles for R-1234ze(E) becomes greater than those for R-134a and R-410A. This can be associated with the discharge temperature and power consumption degradation. Furthermore, both the *COP* augmentation and the gain based on the compression work are zero when $\theta = 0$, which correspond to the conventional vapor compression air conditioner system.

Fig. 8 illustrates the effect of the refrigerant temperature leaving the storage tank on the condenser surface augmentation. The condenser surface augmentation for a system with R-

1234ze(E) increases more rapidly than those with R-134a and R-410A. This can be related directly to the additional heat amount obtained from the storage tank. As shown in Fig. 9, the amount of additional heat absorbed by the refrigerants increases by increasing the refrigerant temperature leaving the storage tank. It was noted that to obtain a high amount of additional heat from the storage tank, the combination of high values of mass flow rate and vapor specific heat, and low value of compressor discharge temperature are required.

Based on Fig. 10, which is a plot of compression ratio degradation as a function of the dimensionless temperature of the refrigerant leaving the storage tank, the variation of the discharge pressure can be calculated with an equation of the form:

$$\frac{P_{d,sol}}{P_{d,conv}} = 1 - \frac{f(\theta)}{100} \tag{39}$$

where

$$f(\theta) = a\theta + b\theta^2 + c\theta^3 \tag{40}$$

Values for constants a, b and c are given in Table. 5, which are determined by curve-fitting with 50 data points for each refrigerant.

8. Conclusions

In order to diminish our dependency on the electricity production, a theoretical investigation on the performance of a vapor compression air conditioner system combined with a solar energy source has been presented. The study is based on the pressure-enthalpy chart. Under the same operating conditions, the results are compared with those from conventional vapor compression systems. The comparison is made using R-1234ze(E), a low *GWP* refrigerant, as an alternative to R-134a and R-410A, which are high *GWP* refrigerants.

The following major conclusions can be extracted:

- The combination of conventional vapor compression air conditioners with solar energy sources increases their *COP*s.
- The general performance of R-1234ze(E) is better than R-134a, which in turn is better than R-410A in terms of discharge temperature and power consumption degradation.
- The *COP* augmentation of a system working with R-1234ze(E) is better than the ones using R-134a and R-410A.
- The gain based on compression work is higher using R-1234ze(E) than using R-134a and R-410A.
- The *COP* augmentation, the condenser surface augmentation and the gain based on compression work for R-134a and R-410A are comparable.
- The system with R-1234ze(E) needs a higher condenser surface augmentation than with R-134a and R-410A.
- Due to its lower discharge temperature and higher mass flow rate, the system with R-1234ze(E) offers higher amount of additional heat obtained from the storage tank.

The general performance of these refrigerants favored the use of R-1234ze(E) in residential and commercial air conditioning systems, and this indicates that R-1234ze(E) would be a suitable alternative for both conventional vapor compression and solar assisted vapor compression air conditioner systems.

Appendix A

The fundamental thermodynamic properties of R-1234ze(E) are given as follows:

Vapor pressure (correlation of Thol and Lemmon. 2016):

$$ln\left(\frac{P_v}{P_c}\right) = \frac{T_c}{T}(-7.5888\theta + 1.9696\theta^{1.5} - 2.0827\theta^{2.2} - 4.1238\theta^{4.6}) \qquad (A.1)$$

Where, $\theta = 1 - T/T_c$.

Liquid density (correlation of Thol and Lemmon. 2016):

$$\frac{\rho_l}{\rho_c} = 1 + 1.1996\theta^{0.27} + 2.2456\theta^{0.7} - 1.7747\theta^{1.25} + 1.3096\theta^{1.9} \qquad (A.2)$$

Vapor density (correlation of Thol and Lemmon. 2016):

$$ln\left(\frac{\rho_v}{\rho_c}\right) = \mathrm{N}_1\theta^{0.24} + \mathrm{N}_2\theta^{0.72} + \mathrm{N}_3\theta^{2.1} + \mathrm{N}_4\theta^{4.8} + \mathrm{N}_5\theta^{9.5} \qquad (A.3)$$

Where, N_1=*-1.0308*, N_2=*-5.0422*, N_3=*-11.5*, N_4=*-37.499 and* N_5=*-77.945*.

Liquid viscosity (correlation of Zhao et al. 2014):

$$\mu_l = \rho_l\left(\sum_{k=0}^{3} N_k T^{t_k} + N_4\left(1 - \frac{T}{T_c}\right)^{1.006}\right) \qquad (A.4)$$

Where, $N_0=-22.77 mm^2/s$, $N_1=-1.42\times10^{-2}\ mm^2/sK$, $N_2=31.235\times10^{-5}\ mm^2/sK^2$, $N_3=-3.114\times10^{-7}\ mm^2/sK^3$ and $N_4=35.059 mm^2/s$.

Vapor viscosity (method of Chung et al. 1988):

$$\mu_v = \mu_k + \mu_p \qquad (A.5)$$

Where,

$$\mu_k = \mu_o\left(\frac{1}{G_2} + a_6 y\right) \quad \text{(A.5a)}$$

$$\mu_p = \frac{36.344(MT_c)^{0.5}}{V_c^{2/3}} a_7 y^2 G_2 exp\left(a_8 + \frac{a_9}{T^*} + \frac{a_{10}}{T^{*2}}\right) \quad \text{(A.5b)}$$

Where,

$$\begin{cases} y = \frac{\rho V_c}{6} \\ G_1 = \frac{1.0-0.5y}{(1-y)^3} \\ G_2 = \frac{a_1\left(1-\frac{exp(-a_4 y)}{y}+a_2 G_1 exp(a_5 y)\right)+a_3 G_1}{a_1 a_4+a_2+a_3} \end{cases} \quad \text{(A.5c)}$$

Constants a_i are linear functions of the acentric factor *w*, the reduced dipole moment μ_τ and the association factor κ, thus:

$$a_i = a_o(i) + a_1(i)w + a_2(i)\mu_\tau^4 + a_3(i)\kappa \quad \text{(A.5d)}$$

The acentric factor for R-1234ze(E) is 0.30855 as given by Akasaka (2010) and the correction factor for hydrogen bonding effect of association substances is given by the following expression:

$$\kappa = 1.04239 - 0.02206\frac{\rho_v}{\rho_c} \quad \text{(A.5e)}$$

Constants $a_o(i)$-$a_3(i)$ for $i = \overline{1.10}$ are given in Table A.1.

The dimensionless dipole moment μ_τ is:

$$\mu_\tau = \frac{131.1\mu}{(V_c T_c)^{0.5}} \tag{A.5f}$$

Where, μ is the dipole moment in Debyes. The viscosity of low-pressure is given by:

$$\mu_o = 26.69 \times 10^{-6} \frac{(MT)^{0.5}}{\sigma^2 \Omega^*} \tag{A.5g}$$

Where, $\sigma = T_c/1.2593$ and Ω^* is the reduced collision integral given by the following expression (Neufeld et al., 1972):

$$\Omega^* = \frac{n_1}{(T^*)^{n_2}} + \frac{n_3}{exp(n_4 T^*)} + \frac{n_5}{exp(n_6 T^*)} + n_7 (T^*)^{n_8} sin(n_9 (T^*)^{n_{10}} + n_{11}) \tag{A.5h}$$

Where, $n_1 = 1.16145$, $n_2 = 0.14874$, $n_3 = 0.52487$, $n_4 = 0.77320$, $n_5 = 2.16178$, $n_6 = 2.43787$, $n_7 = -6.435 \times 10^{-4}$, $n_8 = 0.14874$, $n_9 = 18.0323$, $n_{10} = -0.7683$, $n_{11} = -7.27371$, and $T^* = 1.2593 T_r$ is the dimensionless temperature.

Liquid thermal conductivity (Hasselman and Thomas, 1987; Baroncini et al., 1981):

$$k_l = 0.0361 \frac{T_b^{6/5}}{M T_c^{1/6}} \frac{(1-T_r)^{0.38}}{T_r^{1/6}} \tag{A.6}$$

In which, T_b is the normal boiling at *1 atm*.

Vapor thermal conductivity (Chung et al., 1984; Chung et al., 1988):

$$k_v = \frac{31.2 \mu_o \psi}{M} \left(\frac{1}{G_2} + b_6 y \right) + q b_7 y^2 T_r^{0.5} G_2 \tag{A.7}$$

Where

$$q = 3.586 \times 10^{-3} \left(\frac{T_c}{M}\right)^{0.5} V_c^{2/3} \tag{A.7a}$$

$$\psi = 1 + \alpha \frac{0.215 + 0.28288\alpha - 1.061\beta + 0.26665Z}{0.6366 + \beta Z + 1.061\alpha\beta} \tag{A.7b}$$

$$G_2 = \left(\frac{b_1}{y}\right) \frac{1 - exp(-b_4 y) + b_2 G_1 \exp(b_5 y) + b_3 G_1}{b_1 b_4 + b_2 + b_3} \tag{A.7c}$$

In which, $\alpha = \frac{c_v}{R} - \frac{3}{2}$, $\beta = 0.7862 - 0.7109w + 1.3168w^2$, $Z = 2.0 + 10.5T_r^2$, c_v is the vapor heat capacity and the molar gas constant $R = 8.3144621\, J.mol^{-1}.K^{-1}$ (Mohr et al., 2012). Constants b_1 to b_7 are defined by the following expression:

$$b_i = b_o(i) + b_1(i)w + b_2(i)\mu_\tau^4 + b_3(i)\kappa \tag{A.7e}$$

Constants $b_o(i)$-$b_3(i)$ for $i = \overline{1.7}$ are given in Table A.2.

Liquid and vapor enthalpies (method of Lemmon el al. 2009):

$$h = \tau \mathrm{RT} \left[\left(\frac{\partial \alpha^o}{\partial \tau}\right)_\delta + \left(\frac{\partial \alpha^r}{\partial \tau}\right)_\delta\right] + \delta \left(\frac{\partial \alpha^r}{\partial \delta}\right)_\delta + 1 \tag{A.8}$$

Isochoric heat capacity for both liquid and vapor states (method of Lemmon et al. 2009):

$$c_v = -\tau^2 R \left[\left(\frac{\partial^2 \alpha^o}{\partial \tau^2}\right)_\delta + \left(\frac{\partial^2 \alpha^r}{\partial \tau^2}\right)_\delta\right] \tag{A.9}$$

Isobaric heat capacity for both liquid and vapor states (method of Lemmon et al. 2009):

$$\frac{c_p}{R} = \frac{c_v}{R} + \frac{\left[1+\delta\left(\frac{\partial\alpha^r}{\partial\delta}\right)_\tau - \delta\tau\left(\frac{\partial^2\alpha^r}{\partial\delta\partial\tau}\right)\right]^2}{1+2\delta\left(\frac{\partial\alpha^r}{\partial\delta}\right)_\tau + \delta^2\left(\frac{\partial^2\alpha^r}{\partial\delta^2}\right)_\tau} \tag{A.10}$$

Here, c_p and c_v are in *(J.mol^{-1}K^{-1})*, $\delta = \rho/\rho_c$, $\tau = T_c/T$ and α^o is the ideal-gas Helmholtz-energy equation given by (Thol and Lemmon, 2016):

$$\alpha^o = a_1 + a_2\tau + 3ln\tau + \sum_{k=3}^{4} a_k ln[1 - exp(-b_k\tau)] \tag{A.11}$$

Where, $a_1 = -12.558347537$, $a_2 = 8.7912297624$, $a_3 = -9.3575$, $a_4 = 10.717$, $b_3 = 513/T_c$ and $b_4 = 1972/T_c$.

The common functional form for the Helmholtz-energy equation used in this work is that derived from Thol and Lemmon (2016):

$$\alpha^r(\delta,\tau) = \sum_{k=1}^{5} N_k\delta^{d_k}\tau^{t_k} + \sum_{k=6}^{10} N_k\delta^{d_k}\tau^{t_k}exp(-\delta^{l_k}) + \sum_{k=11}^{16} N_k\delta^{d_k}\tau^{t_k}exp(-\eta_k(\delta - \varepsilon_k)^2 - \beta_k(\tau-\gamma_k)^2) \tag{A.12}$$

The coefficients and exponents of the residual part of Eq. (A.12) are given in Table A.3. Furthermore, the derivatives of the ideal gas Helmholtz-energy, required for the above thermodynamic properties, can be found in the work by Lemmon et al. (2009). Note that, if the fluid is superheated, use a guess of saturated vapor density and, if the fluid is subcooled, use a guess of saturated liquid density.

Appendix B

The relation between the number of tubes per row n_t, the transverse pitch X_t and the exchanger height H is:

$$H = n_t X_t \tag{B.1}$$

The number of tube rows N_r, the longitudinal tube spacing X_l and the flow length L_f are related as:

$$L_f = N_t X_l \tag{B.2}$$

The free-flow area per unit length A'_c and the exchanger frontal area A'_{fr} per unit length are:

$$A'_c = \mathrm{n}_t (X_t - d_o)(1 - F_d t) \tag{B.3}$$

$$A'_{fr} = \mathrm{n}_t X_t \tag{B.4}$$

The fin density F_d has units of fins per unit length. The ratio of free-flow area to frontal area of exchanger σ is then:

$$\sigma = (1 - d_o)(1 - F_d t) \tag{B.5}$$

The finned area per unit length A'_f and the tube outside area per unit length A'_{to} are given by:

$$A'_f = N_r n_t \frac{\pi d_o^2}{2} \left(\frac{4}{\pi} \frac{X_l X_t}{d_o^2} - 1 \right) F_d \tag{B.6}$$

$$A'_{to} = N_r n_t \pi d_o (1 - F_d t) \tag{B.7}$$

The total outside transfer area of exchanger per unit length A'_o is than:

$$A'_o = A'_f + A'_{ot} \tag{B.8}$$

Furthermore, the total inside area of exchanger tubes per unit length A'_i is defined as:

$$A'_i = N_r n_t \pi d_i \tag{B.9}$$

References

Abu Madi, M., Johns, R.A., Heikal, M.R., 1998. Performance characteristics correlation for round tube and plate finned heat exchangers. Int. J. Refrig. 21 (7), 223-230.

Aisbett, E.K., Pham, Q.T., 1998. Natural replacements for ozone-depleting refrigerants in eastern and southern Asia. Int. J. Refrig. 21 (1), 18–28.

Akasaka, R., 2010. An application of the extended corresponding states model to thermodynamic property calculations for trans-1,3,3,3-tetrafluoropropene (HFO-1234ze(E). Int. J. Refrig. 33, 907–914.

Al-Alili, A., Hwang, Y., Radermacher, R., Kubo, I., 2012. A high efficiency solar air conditioner using concentrating photovoltaic/thermal collectors. Appl. Energ. 93, 138-147.

Al-Alili, A., Hwang, Y., Radermacher, R., 2014. Review of solar thermal air conditioning technologies. Int. J. Refrig. 39, 4-22.

Ansari, N.A., Yadav, B., Kumar, J., 2013. Theoretical exergy analysis of HFO-1234yf and HFO-1234ze as an alternative replacement of HFC-134a in simple vapour compression refrigeration system. Int. J. Sci. Eng. Res. 4 (8), 137-144.

Aprea, C., Greco, A., Maiorino, A., 2016. An experimental investigation on the substitution of HFC134a with HFO1234yf in a domestic refrigerator. Appl. Therm. Eng. 106, 959–967.

Arora, S., Chitkara, S., Udayakumar, R., Ali, M., 2011. Thermal analysis of evacuated solar tube collectors. J. Petroleum. Gas. Eng. 2 (4), 74-82.

Babiloni, A.M., Esbri, J.N., Barragan, A., Molés, F., Peris, B., 2014. Drop-in energy performance evaluation of R1234yf and R1234ze(E) in a vapor compression system as R134a replacement. Appl. Therm. Eng. 71, 259–265.

Baroncini, C., Di Filippo, P. Latini, G., Pacetti, M., 1981. Organic liquid thermal conductivity: a prediction method in the reduced temperature range 0.3 to 0.8. Int. J. Thermophys. 2 (1), 21–38.

Bejan, A., 1989. Theory of heat transfer-irreversible refrigeration plants. Int. J. Heat. Mass. Tran. 32 (9), 1631–1639.

Benning, A.F., McHarness, R.C., 1939. Thermodynamic properties of fluorochloromethanes and –ethanes. Ind. Eng. Chem. 31 (7), 912–916.

Bhatkar, V.W., Kriplani, V.M., Awari, G.K., 2013. Alternative refrigerants in vapor compression refrigeration cycle for sustainable environment: a review of recent research. Int. J. Environ. Sci. Te. 10, 871–880.

Bilgili, M., 2011. Hourly simulation and performance of solar electric-vapor compression refrigeration system. Sol. Energy. 85, 2720–2731.

Bitzer,. 2014. New F-Gas Regulation-Consequences. Bitzer Kühlmaschinenbau GmbH, Subject to change.

Bivens, D.B., Yokozeki, A., 1994. Heat transfer coefficient and transport properties for alternative refrigerants. In: Int. Refrig. and Air Cond. Conf. at Purdue, West Lafayette, IN, USA, Paper No. 263.

Bourabaa, A., Saighi, M., Belal, I., 2011. The influence of the inlet conditions on the air side heat transfer performance of plain finned evaporator. In: World. Acad. Sci. Eng. and Technol. 59, Paris, France.

Brown, J. S., Motta, S.F.Y., Domanski, P. A., 2002. Comparative analysis of an automotive air conditioning systems operating with CO2 and R134a. Int. J. Refrig. 25, 19-32.

Bryson, M., Dixon, C., Hill, S.S., 2011. Testing of HFO-1234yf and R152a as mobile air conditioning refrigerant replacements. Ecolibrium, 30–38.

Calm, J.M., Didion, D.A., 1998. Trade-offs in refrigerant selections: past, present, and future. Int. J. Refrig. 21 (4), 308–321.

Calm, J.M., 2008. The next generation of refrigerants-historical review, considerations, and outlook. Int. J. Refrig. 31, 1123–1133.

Chen, Y., Halm, N.P., Eckhard, A., Groll, A., Braun, J.E., 2002. Mathematical modeling of scroll compressors-part 1: compression process modeling. Int. J. Refrig. 25, 731-750.

Cleland, A.C., 1986. Computer subroutines for rapid evaluation of refrigerant thermodynamic properties. Int. J. Refrig. 9, 346-351.

Cleland, A. C., 1994. Polynomial curve-fits for refrigerant thermodynamic properties: extension to include R134a. Int. J. Refrig. 17 (4), 245-249.

Chung, T.H., Lee, L.L., Starling, K.E., 1984. Applications of kinetic gas theories and multiparameter correlation for prediction of dilute gas viscosity and thermal conductivity. Ind. Eng. Chem. Fundam. 23 (1), 8-13.

Chung, T.H., Ajlan, M., Lee, L.L., Starling, K.E., 1988. Generalized multiparameter correlation for nonpolar and polar fluid transport properties. Ind. Eng. Chem. Res. 27, 671-679.

Devotta, S., Gopichand, S., Pendyala, V.R., 1993. Assessment of HFCs, fluorinated ethers and amine as alternatives to CFC12. Int. J. Refrig. 16 (2), 84–90.

Devotta, S., 1995. Alternative heat pump working fluids to CFCs. Heat. Recov. Syst. 15 (3), 273-279.

Devotta, S., Waghmare, A.V,. Sawant, N.N., Domkundwar, B.M., 2001. Alternatives to HCFC-22 for air conditioners. Appl. Therm. Eng. 21, 703–715.

Dinçer, I., Rosen, M.A., 2011. Thermal Energy Storage: Systems and Applications. second Ed. John Wiley and Sons, Chichester, UK.

Dittus, F.W., Boelter L.M.K.,1985. Heat transfer in automobile radiators of the tubular type. Int. Commun. Heat. Mass. 12, 3-22.

Esbri, J.N., Miranda, J.M.M., Babiloni, A.M., Cervera, A.B., Flores, J.M.B., 2013. Experimental analysis of R1234yf as a drop-in replacement for R134a in a vapor compression system. Int. J. Refrig. 36, 870-880.

EU., 2014. Regulation (EU) No 517/2014 of the European Parliament and of the Council of 16 April 2014, on fluorinated greenhouse gases and repealing Regulation (EC). No 842/2006, Official Journal of the European Union, April.

Fernandez, A.I., Martinez, M., Segarra, M., Martorell, I., Cabeza, L.F., 2010. Selection of materials with potential in sensible thermal energy storage. Sol. Energ. Mat. C. 94, 1723-1729.

Godwin, D.S., 1994. Results of soft-optimized system tests in ARI's R-22 alternative refrigerants evaluation program. In: Int. Refrig. and Air Cond. Conf. at Purdue, West Lafayette, IN, USA, Paper No. 217.

Ha, Q.P., Vakiloroaya, V., 2012. A novel solar-assisted air-conditioner system for energy savings with performance enhancement. Procedia. Eng. 49, 116–123.

Ha, Q. P., Vakiloroaya, V., 2015. Modeling and optimal control of an energy-efficient hybrid solar air conditioning system. Automat. Constr. 49, 262–270.

Hasselman, D.P.H., Thomas, J.R., 1987. Thermal Conductivity. Plenum Press, 20, New York and London.

Hendricks, J.Q., 1953. Industrial fluoro-chemicals. Ind. Eng. Chem. 45 (1), 99–105.

Henning, H.M., 2007. Solar assisted air conditioning of buildings-an overview. Appl. Therm. Eng. 27, 1734-1749.

Hong, K.T., Webb, R.L., 1996. Calculation of fin efficiency for wet and dry fins. HVAC & R Res. 2 (1), 27-41.

Janicki, C., Hermann, K., Neumann, J., Riley, P., Mathison, M.M., 2014. Performance of an R-410A room air conditioner modified for use with R-1234ze. In: Int. Refrig. and Air Cond. Conf. at Purdue, West Lafayette, IN, USA, Paper No. 1534.

Kabelac, S., 1991. A simple set of equations of state for process calculations and its application to R134a and R152a. Int. J. Refrig. 14, 217-222.

Kalogirou, S.A., 2004. Solar thermal collectors and applications. Prog. Energ. Combust. 30, 231-295.

Karber, K.M., Abdelaziz, O., Vineyard, E.A., 2012. Experimental performance of R-1234yf as drop-in replacement for R-134a in domestic refrigerators. In: Int. Refrig. and Air Cond. Conf. at Purdue, West Lafayette, IN, USA, Paper No. 1228.

Kayansayan, N.,1994. Heat transfer of plate fin-tube heat exchangers. Int. J. Refrig. 17 (1), 49-57.

Klein, S.A., 1992. Design considerations for refrigeration cycles. Int. J. Refrig. 15 (3), 181–185.

Klein, S.A., Reindl, D.T., 1998. The relationship of optimum heat exchanger allocation and minimum entropy generation rate for refrigeration cycles. J. Energ. Resour. 120, 172–178.

Kraus, R., Strathmann, J.L., Sengers, J.V., Stephan, K., 1993. Transport properties of 1,1,1,2-tetrafluoroethane (R134a). Int. J. Thermophys. 14 (4), 951–988.

Küçüksille, E.U., Selbas, R., Sencan, A., 2009. Data mining techniques for thermophysical properties of refrigerants. Energ. Convers. Manage. 50, 399-412.

Küçüksille, E.U., Selbas, R., Sencan, A., 2011. Prediction of thermodynamic properties of refrigerants using data mining. Energ. Convers. Manage. 52, 836-848.

Leff, H.S., 1987. Thermal efficiency at maximum work output: new results for old heat engines. Am. J. Phys. 55 (7), 602-610.

Leck, T.J., 2009. Evaluation of HFO-1234yf as a potential replacement for R-134a in refrigeration applications. 3rd Conf. Therm. Prop. and Tran. Proc. of Refrigerants, Boulder, CO, USA, Paper No. 155.

Leck, T.J., 2010. New high performance, low GWP refrigerants for stationary AC and refrigeration. In: Int. Refrig. and Air Cond. Conf. at Purdue, West Lafayette, IN, USA, Paper No. 1032.

Leland, T.W., Chappelear, P.S., 1968. The corresponding states principle: a review of current theory and practice. Ind. Eng. Chem. 60 (7), 15-43.

Lemmon, E.W., 2003. Pseudo-pure fluid equations of state for the refrigerant blends R-410A, R-404A, R-507A, and R-407C. Int. J. Thermophys. 24 (4), 991-1006.

Lemmon, E.W., Huber, M.L., McLinden, M.O., 2007. Reference fluid thermodynamic and transport properties-REFPROP, Version 8.0. In: NIST Standard Reference Database 23.

Lemmon, E.W., McLinden, M.O., Wagner, W., 2009. Thermodynamic properties of pressure. III. A reference equation of state for temperatures from the melting line to 650 K and pressures up to 1000 MPa. J. Chem. Eng. Data. 54, 3141-3180.

London, A.L., Seban, R.A., 1980. A generalization of the methods of heat exchanger analysis. Int. J. Heat. Mass. Tran. 23, 5-16.

Lottin O., Guillement, P., Lebreton, J.M., 2003. Effects of synthetic oil in a compression refrigeration system using R410A. Part I: modelling of the whole system and analysis of its response to an increase in the amount of circulating oil. Int J Refrig. 26, 772-782.

McLinden, M.Q., Didion, D.A., 1988. The search for alternative refrigerant – a molecular approach. In: Int. Refrig. and Air Cond. Conf. at Purdue, West Lafayette, IN, USA, Paper No. 69.

McQuiston, F.C., 1980. Finned tube heat exchangers: state of the art for the air side. In: 5th Annu. Heat. Pump. Technol. Conf. at Oklahoma State University, Oklahoma, USA, 1980.

McQuiston, F.C., Parker, D.A., 1982. Heating, Ventilating and Air Conditioning: Analysis and Design, second Ed. John Wiley and Sons, New York.

Meng, Z., Zhang, H., Qiu, J., Lei, M., 2016. Theoretical analysis of R1234ze(E), R152a, and R1234ze(E)/R152a mixtures as replacements of R134a in vapor compression system. Adv. Mech. Eng. 8 (11), 1-10.

Michel, B., Mazet, N., Mauran, S., Stitou, D., Xu, J., 2012. Thermochemical process for seasonal storage of solar energy: characterization and modeling of a high density reactive bed. Energy. 47, 553-563.

Midgley, T., Henne, A.L., 1930. Organic fluorides as refrigerants. Ind. Eng. Chem. 22 (5), 542–545.

Minor, B., Spatz, M., 2008. HFO-1234yf low GWP refrigerant update. In: Int. Refrig. and Air Cond. Conf. at Purdue, West Lafayette, IN, USA, Paper No. 937.

Missoum, M., Hamidat, A., Loukarfi, L., Abdeladim, K., 2014. Impact of rural housing energy performance improvement on the energy balance in the North-West of Algeria. Energ. Buildings. 85, 374–388.

Mohr, P. J., Taylor, B. N., Newell, D. B., 2012. CODATA recommended values of the fundamental physical constants: 2010. Rev. Mod. Phys. 84 (4), 1527-1605.

Motta, S.F.Y., Domanski, P.A., 2000. Performance of R-22 and its alternatives working at high outdoor temperatures. In: Int. Refrig. and Air Cond. Conf. at Purdue, West Lafayette, IN, USA, Paper No. 464.

Motta, S.F.Y., Bercerra, E.D.V., Spatz, M.W., 2010. Analysis of LGWP alternatives for small refrigeration (plugin) applications. In: Int. Refrig. and Air Cond. Conf. at Purdue, West Lafayette, IN, USA, Paper No. 1149.

Neufeld, P. D., Janzen, A. R., Aziz, R. A., 1972. Empirical equations to calculate 16 of the transport collision integrals $\Omega^{(l,s)*}$ for the Lennard-Jones (12-6) potential. J. Chem. Phys. 57 (3), 1100-1102.

Nielsen, O.J., Javadi, M.S., Andersen, M.P.S., Hurley, M.D., Wallington, T.J., Singh, R., 2007. Atmospheric chemistry of $CF_3CF=CH_2$: kinetics and mechanisms of gas-phase reactions with Cl atoms, OH radicals, and O_3. Chem. Phys. Lett. 439, 18-22.

Papadimitriou, V.C., Talukdar, R.K., Portmann, R.W., Ravishankara, A.R., Burkholder, J.B., 2008. $CF_3CF=CH_2$ and (Z)-$CF_3CF=CHF$: temperature dependent OH rate coefficients and global warming potentials. Phys. Chem. Chem. Phys. 10, 808-820.

Pham, H., Rajendran, R., 2012. R32 and HFOs as low-GWP refrigerants for air conditioning. In: Int. Refrig. and Air Cond. Conf. at Purdue, West Lafayette, IN, USA, Paper No. 2262.

Rabas, T. J., Eckels, P. W., Sabatino, R. A., 1981. The effect of fin density on the heat transfer and pressure drop performance of low-finned tube banks. Chem. Eng. Commun. 10, 127-147.

Radcenco, V., Vargas, J.V.C., Bejan, A., Lim, J.S., 1995. Two design aspect of defrosting refrigerators. Int J Refrig. 18 (2), 76-86.

Rojas, D., Beermann, J., Klein, S.A., Reindl, D.T., 2008. Thermal performance testing of flat-plate collectors. Sol. Energy. 82, 746-757.

Saechan, P., Wongwises, S., 2008. Optimal configuration of cross flow plate finned tube condenser based on the second law of thermodynamics. Int. J. Therm. Sci. 47, 1473-1481.

Shah, M.M., 1979. A general correlation for heat transfer during film condensation inside pipes. Int. J. Heat. Mass. Tran. 22, 547-556.

Shah, M.M.. 2009. An improved and extended general correlation for heat transfer during condensation in plain tubes. HVAC & R Res. 15(5), 889-913.

Sharma, A., Tyagi, V.V., Chen, C.R., Buddhi, D., 2009. Review on thermal energy storage with phase change materials and applications. Renew. Sust. Energ. Rev. 13, 318-345.

Spatz, M.W., Motta, F.S.Y., 2004, An evaluation of options for replacing HCFC-22 in medium temperature refrigeration systems. Int. J. Refrig. 27, 475-483.

Tatsidjodoung, P., Pierrès, N.L., Luo, L., 2013. AA review of potential materials for thermal energy storage in building applications. Renew. Sust. Energ. Rev. 18, 327-349.

Thol, M., Lemmon, E.W., 2016. Equation of state for the thermodynamic properties of trans-1,3,3,3-tetrafluoropropene [R-1234ze(E)]. Int. J. Thermophys. 37 (3), 1-16.

Tobin, M.C., 1969. Engine efficiencies and the second law of thermodynamics. Am. J. Phys. 37 (11), 1115-1117.

Trepp, Ch., Savoie, P., Kraus, W.E., 1992. Investigation of the performance behaviour of a compression refrigerating unit with halogen refrigerant mixtures R22/R142b, R22/R114 and R22/R12. Int. J. Refrig. 15 (2), 101–111.

Vakiloroaya, V., Ha, Q. P., Skibniewski, M., 2013. Modeling and experimental validation of a solar-assisted direct expansion air conditioning system. Energ. Buildings. 66, 524–536.

Wang, C.C., Chang, Y.J., Hsieh, Y.C., Lin, Y.T., 1996. Sensible heat and friction characteristics of plate fin-and-tube heat exchangers having plane fins. Int. J. Refrig. 19 (4), 223-230.

Wang, C.C., Chi, K.Y., Chang, C.J., 2000. Heat transfer and friction characteristics of plain fin-and-tube heat exchangers, part II: correlation. Int. J. Heat. Mass. Tran. 43, 2693-2700.

Webb, R.L., 1980. Air-side heat transfer in finned tube heat exchangers. Heat. Transf. Eng. 1 (3), 33-49.

Wu, C., 1995. Maximum obtainable specific cooling load of a refrigerator. Energ. Convers. Manage. 36 (1), 7–10.

Wu, C., Chen, L., Sun, F., 1996. Optimization of steady flow refrigeration cycles. Int. J. Ambient. Energy. 17 (4), 199–206.

Xu, X., Hwang, Y., Radermacher, R., 2013. Performance comparison of R410A and R32 in vapor injection cycles. Int. J. Refrig. 36, 892–903.

Zambolin, E., Del Col, D., 2010. Experimental analysis of thermal performance of flat plate and evacuated tube solar collectors in stationary standard and daily conditions. Sol. Energy. 84, 1382-1396.

Zhao, G., Bi. S., Fröba, A.P., Wu, J., 2014. Liquid viscosity and surface tension of R1234yf and R1234ze under saturation conditions by surface light scattering. J. Chem. Eng. Data. 59, 1366-1371.

Table. 1 Critical properties reported for the selected refrigerants

Properties	R-134a (Kraus et al., 1993)	R-410A (Xu et al., 2013)	R-1234ze(E) (Akasaka, 2010)
Chemical formula	CH_2FCF_3	$CH2F_2/CHF_2CF_3$	Trans-$CHF=CHCF_3$
Molar mass, M *(g.mol^{-1})*	102.03	72.60	114.04
Critical temperature, T_c *(°C)*	101.12	72.10	109.36
Critical pressure, P_c *(MPa)*	4.065	4.930	3.632
Critical density, ρ_c *(kg.m^{-3})*	515.25	489.00	486.00
Normal boiling point, *(°C)*	-26.06	-51.50	-19.232
Critical volume, V_c *(m^3.kg^{-1})*	0.00194	0.00204	0.00206

Table. 2 Geometric dimensions of the fin-and-tube condenser

parameter	Dimension
Tube outside diameter, d_o *(mm)*	8.62
Fin pitch, F_p *(mm)*	1.20
Fin thickness, t *(mm)*	0.115
Longitudinal tube pitch, X_l *(mm)*	22.0
Transverse tube pitch, X_t *(mm)*	25.4
Number of tube rows, N_r *(-)*	2
Number of tubes per row, n_t *(-)*	12
Ratio of free-flow to frontal area, σ *(-)*	0.597

Table. 3 Calculated parameters for conventional vapor compression air conditioner

Parameters	R-134a	R-410A	R-1234ze(E)
Refrigerant mass flow rate, m_r *(kg.s^{-1})*	0.0228	0.0206	0.0245
Latent heat of evaporation, h_{fg}^{e} *(kJ.kg^{-1})*	198.60	221.31	189.34
Latent heat of condensation, h_{fg}^{c}, *(kJ.kg^{-1})*	163.02	158.93	159.85
Enthalpy at evaporator inlet, h_4 *(kJ.kg^{-1})*	248.92	256.64	246.11
Enthalpy difference, $(\Delta h)^{e}$, *(kJ.kg^{-1})*	154.17	170.35	143.54
Isentropic discharge temperature, $T_{d,is}$ *(°C)*	50.5	59.7	42.0
Actual discharge temperature, $T_{d,act}$ *(°C)*	57.6	71.3	47.0
Evaporating pressure, P_{sat}^{e} *(10^5 Pa)*	2.928	7.981	2.166
Condensing pressure, P_{sat}^{e} *(10^5 Pa)*	10.166	24.187	7.665
Power required for isentropic compressor, w_{is} *(W)*	648.0	715.1	634.6
Power required for actual compressor, w_{act} *(W)*	832.0	1156.6	723.2
Heat transfer rate in desuperheated region, Q_{des}^{c}, *(W)*	459.2	1192.4	255.2
Heat transfer rate in two-phase region, Q_{tp}^{c} *(W)*	3719.1	3281.4	3917.0
Heat transfer rate in subcooled region, Q_{sub}^{c} *(W)*	170.9	200.2	186.9
Total heat transfer rate, Q^{c} (W)	4349.2	4673.8	4359.0
Condensing heat transfer coefficient, α_{tp}^{c} *(W.m^{-2}.K^{-1})*	5488.2	3844.0	4869.6
Condenser tube length, L^{c} *(m)*	0.9647	0.9691	0.8963
Coefficient of performance, COP *(-)*	4.22	3.04	4.55
Isentropic efficiency, η_{is} *(-)*	0.78	0.62	0.82
Compression index, c *(-)*	1.17	1.34	1.13
Pressure ratio, P_r *(-)*	3.47	3.03	3.54

Table. 4 Calculated parameters for conventional vapor compression air conditioner with solar collector

Parameters	R-134a	R-410A	R-1234ze(E)
Refrigerant temperature leaving storage tank, *(°C)*	85	85	85
Isentropic discharge temperature, $T_{d,is}$ *(°C)*	43.3	53.5	35.9
Actual discharge temperature, $T_{d,act}$ *(°C)*	49.0	63.5	39.9
Isentropic discharge pressure, $P_{d,is}$ *(10^5 Pa)*	8.981	22.058	6.613
Actual discharge pressure, $P_{d,act}$ *(10^5 Pa)*	9.088	22.461	6.675
Power required for isentropic compressor, w_{is} *(W)*	578.1	647.7	565.5
Power required for actual compressor, w_{act} *(W)*	725.4	1026.1	641.9
Heat transfer rate in desuperheated region, Q^c_{des}, *(W)*	1231.0	1877.1	1213.2
Additional heat absorbed in storage tank *(W)*	771.9	684.8	958.0
Condenser tube length, L^c *(m)*	0.9789	0.9822	0.9187
Coefficient of performance, COP *(-)*	4.85	3.43	5.48
Isentropic efficiency, η_{is} *(-)*	0.80	0.63	0.86
Condenser surface augmentation, *(%)*	1.50	1.40	2.50
Compression ratio degradation, *(%)*	11.66	8.80	13.58
COP augmentation, *(%)*	14.70	12.72	20.45
Gain based on isentropic work, *(%)*	10.80	9.43	12.30
Gain based on actual work, *(%)*	12.82	11.28	16.98

Table. 5 Constants used in Eq. (40)

Constant	R-134a	R-410A	R-1234ze(E)
a	18.491	15.074	20.988
b	-2.762	-1.796	-3.754
c	0.323	0.175	0.506

Table A. 1 Constants used in Eq. (A.5d) (Chung et al., 1988)

i	$a_o(i)$	$a_1(i)$	$a_2(i)$	$a_3(i)$
1	6.32402	50.41190	-51.68010	1189.02000
2	0.12102×10^{-2}	-1.1536×10^{-3}	-6.255710×10^{-3}	3.72830×10^{-2}
3	5.28346	254.20900	-168.48100	3898.27000
4	6.62263	38.09570	-8.46414	31.41780
5	19.74540	7.63034	-14.35440	31.52670
6	-1.89992	-12.53670	4.98529	-18.15070
7	24.27450	3.44945	-11.29130	69.34660
8	0.79716	1.11764	1.23480×10^{-2}	-4.11661
9	-0.23816	6.76950×10^{-2}	0.81630	4.02528
10	6.8629×10^{-2}	0.34793	0.59256	-0.72663

Table A. 2 Constants used in Eq. (A.7e) (Chung et al., 1988)

i	$b_o(i)$	$b_1(i)$	$b_2(i)$	$b_3(i)$
1	2.41657	0.74824	-0.91858	121.72100
2	-0.50924	-1.50936	-49.99120	69.98340
3	6.61069	5.62073	64.75990	27.03890
4	14.54250	-8.91387	-5.63794	74.34350
5	0.79274	0.82019	-0.69369	6.31734
6	-5.86340	12.80050	9.58926	-65.52920
7	81.17100	114.15800	-60.84100	466.77500

Table A. 3 Constants used in Eq. (A.12) (Thol and Lemmon, 2016)

k	N_k	t_k	d_k	l_k	η_k	β_k	γ_k	ε_k
1	0.03982797	1.000	4	-	-	-	-	-
2	1.81222700	0.223	1	-	-	-	-	-
3	-2.53751200	0.755	1	-	-	-	-	-
4	-0.53332540	1.240	2	-	-	-	-	-
5	0.16770310	0.440	3	-	-	-	-	-
6	-1.32380100	2.000	1	2	-	-	-	-
7	-0.66946540	2.200	3	2	-	-	-	-
8	0.80727180	1.200	2	1	-	-	-	-
9	-0.77402290	1.500	2	2	-	-	-	-
10	-0.01843846	0.900	7	1	-	-	-	-
11	1.40791600	1.330	1	-	1.00	1.21	0.943	0.728
12	-0.42370820	1.750	1	-	1.61	1.37	0.642	0.870
13	-0.22705213	2.110	3	-	1.24	0.98	0.590	0.855
14	-0.80521300	1.000	3	-	9.34	171.00	1.200	0.790
15	0.00994318	1.500	2	-	5.78	47.40	1.330	1.300
16	-0.008798793	1.000	1	-	3.08	15.40	0.640	0.710